International Journal of Maritime Engineering

EFFECT OF THE SPANWISE DISCRETISATION ON TURBULENT FLOW PAST A CIRCULAR CYLINDER

S Kim, P A Wilson and **Z Chen,** University of Southampton, UK

SUMMARY

The effect of the spanwise discretisation on numerical calculations of the turbulent flow around a circular cylinder is systematically assessed at a subcritical Reynolds number of 10000 in the frame of three-dimensional large-eddy simulation. The eddy-viscosity k-equation subgrid scale model is implemented to evaluate unsteady turbulent flow field. Large-eddy simulation is known to be a reliable method to resolve such a challenging flow field, however, the high computational efforts restrict to low Reynolds number flow or two-dimensional calculations. Therefore, minimum spatial density in the spanwise direction or cylinder axis direction needs to be carefully evaluated in order to reduce high computational resources. In the present study, the influence of the spanwise resolutions to satisfactorily represent three-dimensional complex flow features is discussed in detail and minimum spatial density for high Reynolds flow is suggested.

1. INTRODUCTION

Since most of structural members are designed as the shape of the circular cylinder in upstream industries, the accurate numerical simulation of the bluff body flow is a highly demanding application. Among various simulation methodologies, nowadays, large-eddy simulation (LES) technique tends to be increasingly applied for which the Reynolds-Averaged Navier-Stokes (RANS) approach is incapable of accurately predicting unsteady hydrodynamic forces acting on the body in harsh ocean environment, which is mostly attributed to the significant increase in high performance computing (HPC) capacity.

Many LESs have been conducted for the turbulent flow over a circular cylinder especially at Reynolds number of 3900, mainly due to available experimental results at the Reynolds number. [1] is of the first to conduct LES calculation at the canonical Reynolds number. Several other researchers have examined a variety of aspects that affect the quality of LES solutions of the cylinder flow as well. In the three-dimensional (3-D) numerical investigations including [2,3,4], the effects of the subgrid scale (SGS) models and discretisation schemes especially for the convective flux have been widely examined at Re=3900. In general, the central difference (CD) schemes are observed to produce better reliable numerical solutions compared with the experimental data than upwind class schemes.

In most of the previous numerical studies, the cylinder spanwise length to diameter ratio equal to $L_Z/D = \pi$ was adopted in order to predict three-dimensionality of the cylinder wake together with a number of control volumes $N_Z = 32$ and 48, e.g. see recent works by [5,6]. The minimum spanwise extension of the computational domain was clearly assessed with three different spanwise lengths, $\pi/2$, π and 2π [7]. Whilst the spanwise length $L_Z = \pi D$ is severely shorter than the length used in the experiments, the representative cylinder section with the characteristic spanwise length seems to be enough to predict the three-dimensionality of the cylinder flow in general. However, the length could be properly increased when the lift force is in local minimum as indicated in [8,9].

In the LES study conducted by [3], the influence of the spanwise resolution was examined at Re=3900 as well. Their numerical results obtained from different grid densities with $N_Z = 32$ and 64 along the spanwise domain length $L_Z = \pi D$ exhibited quite different behaviours of the force coefficients and turbulent kinetic energy, and the important role of the resolution in the cylinder axis direction was emphasised. In a previous study by the authors [10] the 3-D cylinder flow at Re=5500 was examined and the predicted wake parameters such as unsteady lift obtained from the conventional Smagorinsky SGS model on the high grid density in the spanwise direction $N_Z = 96$ showed a close approximation compared to the experimental data measured by [9]. However, the numerical solution was quite expensive in terms of computational cost.

Recent efforts at higher Reynolds numbers have focused on the effects of various SGS and wall damping models. The pioneering LES simulation was conducted by [11] at Re=140000 with two different SGS models. The predicted flow quantities from the algebraic Smagorinsky model were in satisfactory agreement with the experimental data, compared to those obtained from the dynamic model. This study at the practical Reynolds number showed that the superiority of the dynamic model over the conventional Smagorinsky model was not proved with exception that no proper model constant has to be chosen in the dynamic model. An interesting result from this study at the high Reynolds number flow is that the grid refinement did not automatically lead to improved numerical solutions compared to the experiments. In a recent numerical investigation using 3-D LES with a wall-adapting local eddy-viscosity (WALE) SGS model at Re=3900, 10000 and 20000 [12], the wake parameters were calculated reasonably well at the lower Reynolds number of 3900,

while the results are over-predicted at the higher ends of the Reynolds numbers and the flow statistics were not reported.

In order to achieve close approximations with experiments at practical or high Reynolds numbers, various computational parameters, which strongly influence on the numerical solutions, should be carefully chosen and properly implemented, e.g. grid density, discretisation scheme, domain size and SGS turbulence modelling. Among those factors, the aspect ratio of cylinder length to diameter L_Z/D and SGS modelling has been widely examined in the literature. However, to the authors' knowledge, the effect of the spanwise discretisation density on the turbulent flow behind the 3-D bluff body at high Reynolds number are not systematically evaluated and it has often been underestimated for 3-D LES due to limitation of computer resources.

The aim of the present study is, therefore, to examine turbulent flow behind a circular cylinder at Re=10000 and determine the influence of the spatial resolution in the spanwise direction on 3-D LES solutions. By carrying the solutions to different spanwise densities and visualising the averaged flow statistics behind the cylinder, the effect of the spanwise discretisation resolution will be evaluated. It will then be possible to determine the minimum spanwise density reasonably, which is required to capture 3-D unsteady turbulent flow along a circular cylinder axis for high Reynolds number flow.

2. COMPUTATIONAL MODELLING

2.1 FLOW MODELLING APPROACH

LES technique is employed for 3-D time-dependent flow of an incompressible and viscous fluid around a circular cylinder. The LES equations are derived from the Navier-Stokes equations using the predefined filter kernel $G = G(x, \Delta)$ in which Δ is the grid filter width. In the spatially filtered Navier-Stokes equations, the subgrid stress tensor τ_{ij} is expressed based on the Boussinesq's assumptions:

$$\tau_{ij} - \frac{2}{3}k_t\delta_{ij} = -2\upsilon_t\left(\bar{S}_{ij} - \frac{1}{3}\bar{S}_{kk}\delta_{ij}\right), \quad (1a)$$

$$\bar{S}_{ij} = \frac{1}{2}\left(\frac{\partial \bar{u}_i}{\partial x_j} + \frac{\partial \bar{u}_j}{\partial x_i}\right), \quad (1b)$$

where $\bar{S}_{ij}$ is the rate of strain tensor computed from the resolved scales. υ_t and k_t are SGS viscosity and turbulent kinetic energy respectively.

In the present study, the k-equation SGS model [13] is implemented in order to evaluate turbulent flow field. A comprehensive review of the eddy-viscosity type model is explained in detail by [14]. An advantage of the algebraic k-equation model is that no equilibrium assumption is required, but uses an additional transport equation in order to estimate k_t:

$$\frac{\partial k_t}{\partial t} + \frac{\partial(\bar{u}_j k_t)}{\partial x_j} = P + \frac{\partial}{\partial x_j}\left[(\upsilon + \upsilon_t)\frac{\partial k_t}{\partial x_j}\right] - \epsilon, \quad (2a)$$

$$P = -2\upsilon_t\bar{S}_{ij}\bar{S}_{ij},\ \epsilon = C_\epsilon k_t^{3/2}\Delta^{-1},\ \upsilon_t = C_k\Delta k_t^{0.5}, \quad (2b)$$

where the viscous dissipation ϵ is take to be proportional to $k_t^{3/2}$. The dimensionless model constants are set equal to $C_\epsilon = 1.00$ and $C_k = 0.05$ suggested by [14].

2.2 NUMERICAL SET-UP

The computational domain is the classical O-type with outer boundary 15 cylinder diameters $15D$ from the cylinder centre and the spanwise length $L_Z = \pi D$, which is based on careful previous numerical studies of the cylinder flows, e.g. see [15,16,17]. The hexahedral grid is used to discretise the spatial computational domain. The hexahedral grid is exponentially stretched in the radial direction (r) and is uniformly spaced in the circumferential direction (θ). The resulting non-dimensional distance for the first cells adjacent to the cylinder wall is kept as max. $y^+ \approx 1.0$ to resolve the boundary layer on the cylinder surface in all simulation cases. For the aim of the present study, four different curvilinear grids are generated and Table 1 gives an overview of these different grids, including the corresponding number of control volumes and the non-dimensional grid spacing in the spanwise direction $\Delta z/D$.

Table 1 Grid characteristics.

Case	Resolution $N_r \times N_\theta \times N_z$ [1]	Total cells	y^+_{avg}	$\Delta z/D$
LES-1	$240 \times 240 \times 16$	921,600	0.54	0.20
LES-2	$240 \times 240 \times 32$	1,843,200	0.53	0.10
LES-3	$240 \times 240 \times 64$	3,686,400	0.52	0.05
LES-4	$240 \times 240 \times 96$	5,529,600	0.47	0.04

1) N_z is evenly distributed by the spacing $\Delta z/D$ along cylinder spanwise direction.

A velocity inlet boundary condition is applied and a zero-Neumann condition is used for the outlet. No-slip conditions are imposed to the cylinder surface, whereas periodic boundary conditions are assigned at the spanwise ends.

The finite volume (FV) open source code OpenFoam [18] is used to evaluate the flow field. The cell-centre values of the flow variables are interpolated at face locations using the second-order central differencing scheme for diffusive and convection terms. A second-order implicit Euler method is employed to advance in time. The Pressure-Implicit with Splitting of Operators (PISO) algorithm with a modified Rhie and Chow interpolation is used to deal with the pressure-velocity coupling between the governing equations. A non-dimensional time step

$\Delta tU/D = 0.001$ is used in order to satisfy the temporal resolution requirement of LES in all simulation cases, where U is the free-stream velocity.

The simulation is performed using 112 processors in parallel allowing efficient computation on 2.6 GHz Intel Xeon core and 4GB of memory per core. In general, the CPU time for each simulation case is approximately 200 hours.

3. APPLICATION AND RESULTS

A series of simulations are performed with four different grid densities in conjunction with the k-equation SGS model in order to examine the influence of the spanwise grid density on LES qualities for the subsequent computations. It is worth noticing that instantaneous hydrodynamic coefficients are converged after a non-dimensional time of $\approx 70\, tD/U$. The flow statistics of the integral wake parameters are then compiled for $100\, tD/U$, the mean velocity profiles for $50\, tD/U$ and the mean flow statistics for $70\, tD/U$ as minimum in all simulation cases. All flow data are spanwise-averaged in the homogeneous cylinder axis z-direction.

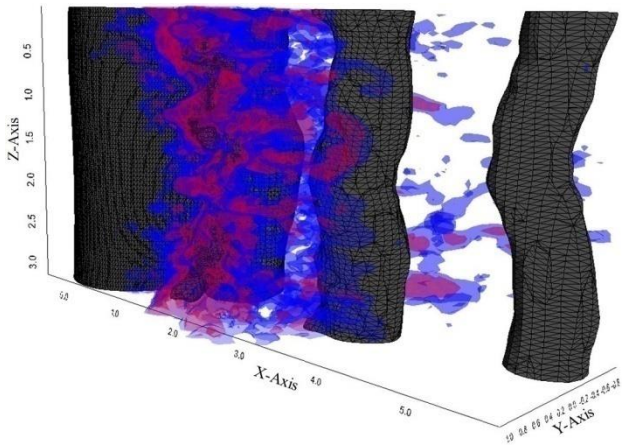

Figure 1: Perspective view of the instantaneous iso-surfaces of pressure and vortices at Re=10000 (LES-3). The cylinder is upstream at left.

Figure 1 illustrates instantaneous iso-surfaces of pressure p and vorticity magnitude $|\omega|$ fields from the case of LES-3. At Reynolds number of 10000, the flow exhibits intense turbulent activity in very near wake around $x/D = 0.5 - 2.0$. The iso-surfaces identify that the pressures which are predominant in the spanwise z-direction are convected further downstream in near wake, and the longitudinal vortices as finger like structures around the pressure cores which originated from the disorganisation in very near wake maintain their coherence further downstream into the streamwise x-direction.

3.1 SENSITIVITY STUDY ON THE MAIN WAKE PARAMETERS

The sensitivity of the main wake parameters to the spanwise discretisation can be evaluated from Table 2. The spanwise resolutions are varied by changing the number of grid in the z-direction, ranging from $N_z = 16$ to 96. As N_z increases, the variation in Strouhal number St is negligible and the relative difference of the mean drag coefficient $\bar{C}_D$ between LES-2 as maximum and LES-4 as minimum is below 5%, indicating that those quantities are generally not too sensitive to the variation of the spanwise resolution. Therefore, the predicted strouhal number and mean drag shows good agreements with the experimental and direct numerical simulation (DNS) data.

In contrast to the drag force, it is pertinent that the relative change of r.m.s. lift coefficient C_L' between LES-2 as maximum and LES-4 as minimum is around 19
% with increasing the spanwise resolution, indicating higher sensitivity on the grid density in the cylinder axis direction. The converged value of the lift in the highest resolution (LES-4) is 0.381 comparable to the value of 0.384 in the experimental measurement [21]. However, it is noted that large scatters about lift coefficient exist

Table 2 Sensitivity study on the main wake parameters at Re=10000: Strouhal number St, mean drag coefficient $\bar{C}_D$, r.m.s. lift coefficient C_L' and mean base suction pressure coefficient $-C_{pb}$.

Case	N_z	St	$\bar{C}_D$	C_L'	$-C_{pb}$
LES-1	16	0.184	1.167	0.438	1.203
LES-2	32	0.208	1.187	0.455	1.206
LES-3	64	0.208	1.149	0.420	1.189
LES-4	96	0.208	1.133	0.381	1.143
LES [12]		0.20	1.22	0.476	-
DNS [19]		0.203	1.143	0.448	1.129
Experiment [20]		-	-	-	1.11
Experiment [21]		0.193	1.186	0.384	-
Empirical formula [9]		0.201	-	0.411	-

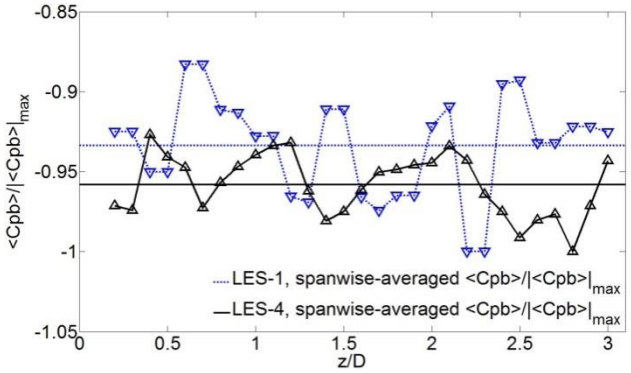

Figure 2: Normalised time-averaged base pressure coefficient $\langle C_{pb}\rangle/\left|\langle C_{pb}\rangle\right|_{max}$ as a function of spanwise distance z/D, showing high fluctuations of pressure along the cylinder axis at Re=10000.

among different experiments [11,19]. As a result, the empirical formula for the lift from a number of the experiments was suggested by [9] and it is generally accepted that the empirical value of 0.411 is a good

representation of lift fluctuations at the considered Reynolds number. Hence, it seems that the predicted lift obtained from LES-4 is at the lower bound of the scatters of the experimental measurements and the lift value from LES-3 shows good agreement with the empirical solution. It is indicated that the spanwise spacing $\Delta z/D \approx 0.05$ is required as minimum spacing in order to predict unsteady lift force reasonably for high Reynolds number flow.

The mean base suction coefficient can be determined as the mean pressure coefficient at the location of the cylinder base. The variation of the coefficient shows the grid independence with increasing N_z as well. The relative change between LES-2 and LES-4 is within 5.5%, but the value from LES-4 is slightly over-predicted compared to the experimental measurement by [20]. Figure 2 shows different behaviours of the normalised mean base pressure coefficients from $\Delta z/D = 0.196$ (LES-1) and 0.037 (LES-4), which emphasise on the influence of the spanwise spacing.

3.2 SENSITIVITY STUDY ON THE MEAN VELOICITY PROFILES

The normalised time-averaged streamwise and transversal velocities, $\langle u \rangle/U$ and $\langle v \rangle/U$, are computed in the near wake of the cylinder. Of course, additional averaging is performed in the spanwise z-direction.

Figure 3 shows the velocity profiles for the mean streamwise velocity along y/D at two different locations, the points of $x/D = 0.6$ around the cylinder base and $x/D = 1.2$ far downstream from the cylinder base. It is clearly seen that the results are distinctively well correlated with each other, but there is a slight shift of the predicted velocities due to the differences of recirculation bubble length obtained from different spanwise resolutions. The overall profiles show a U-shape in very near wake ($x/D = 0.6$) and the profiles evolve towards a V-shape further downstream ($x/D = 1.2$).

The mean crossflow velocity profiles are shown in Figure 4. These transversal velocity components are more affected by the large-scale vortices or Kármán shedding behind the cylinder than the streamwise velocity. In Figure 4(a) the profiles tend to be converged as increasing the spanwise resolution. The profiles with the lower resolution grids (LES-1 and LES-2) demonstrate a higher sensitivity to the resolution, but with the higher resolutions (LES-3 and LES-4) the velocity profiles shows good agreement with each other. At $x/D = 1.4$ as shown in Figure 4(b), the magnitudes of the velocities show larger fluctuations compared those in Figure 4(a) due to the Kármán shedding in the wake.

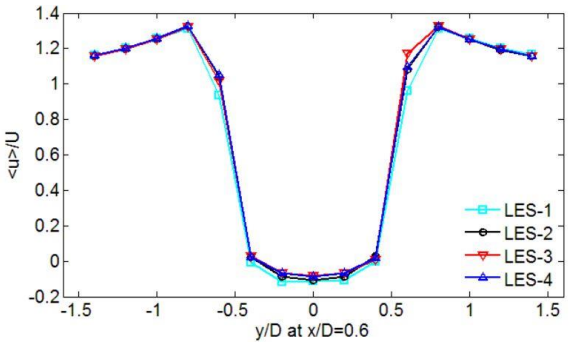

(a) $\langle u \rangle/U$ at $x/D = 0.6$.

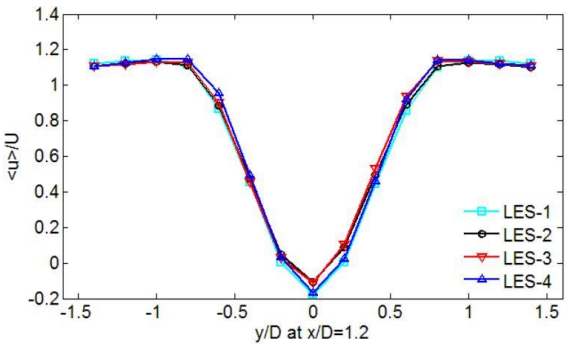

(b) $\langle u \rangle/U$ at $x/D = 1.2$.

Figure 3: The time- and spanwise-averaged streamwise velocity $\langle u \rangle/U$ profiles at two different locations in near wake.

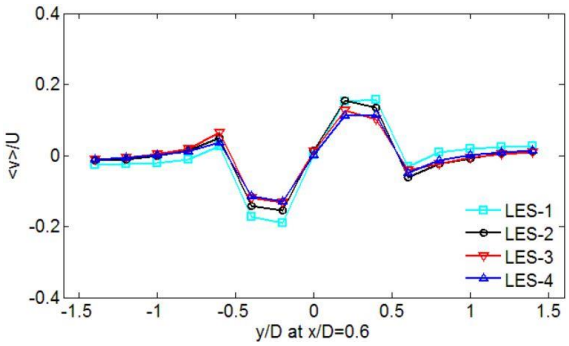

(a) $\langle v \rangle/U$ at $x/D = 0.6$.

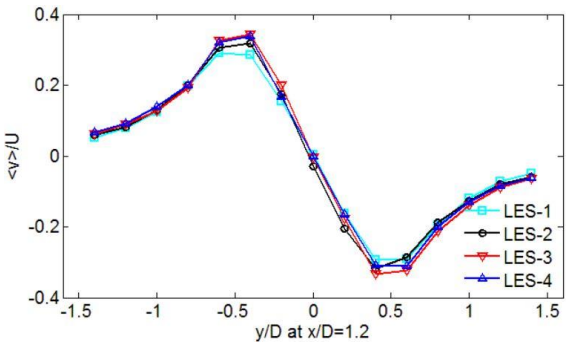

(b) $\langle v \rangle/U$ at $x/D = 1.2$.

Figure 4: The time- and spanwise-averaged crossflow velocity $\langle v \rangle/U$ profiles at two different locations in near wake.

3.3 SENSITIVITY STUDY ON THE MEAN FLOW STATISTICS

Contour plots of the non-dimensional mean velocity $\langle u \rangle / U$ and shear stress $\langle u'v' \rangle / U^2$ predicted in different spanwise grid densities are shown in Figures 5 and 6, where u' and v' are r.m.s. streamwise and crossflow velocities respectively. As a quantitative comparison, Table 3 summarises the computed extreme values of the flow fields, including the experimental and DNS data at Re=10000 [19].

Table 3 Characteristic values of the normalised spanwise-averaged mean components of the velocity and Reynolds stress at Re=10000.

Case		$\langle u \rangle / U$	$\langle u'v' \rangle / U^2$
LES-1 (N_z=16, $\Delta z/D$=0.196)	Peak	-0.28	±0.13
	L_r [1]	1.02D	-
LES-2 (N_z=32, $\Delta z/D$=0.098)	Peak	-0.29	±0.16
	L_r	0.85D	-
LES-3 (N_z=64, $\Delta z/D$=0.049)	Peak	-0.26	±0.17
	L_r	0.80D	-
LES-4 (N_z=96, $\Delta z/D$=0.037)	Peak	-0.30	±0.15
	L_r	0.91D	-
DNS [19]	Peak	-0.249	±0.15
	L_r	0.82D	-
PIV experiment [19]	Peak	-0.228	±0.14
	L_r	0.78D	-

1) The recirculation bubble length L_r of reverse flow or negative velocity in the cylinder wake.

In Figure 5(a-d) the well-defined bubble of negative velocities behind the cylinder are clearly captured in all spanwise resolutions. The predicted minimum peak values of the streamwise velocities in all simulation cases are ranging from -0.26 to -0.30 with a small relative change of about 6.5%. However, the length of the recirculation bubble, from the cylinder base to the location at zero velocity, is highly dependent on the resolution. As N_z increases from 16 to 64, the characteristic length is sharply decreased by about 21% and the predicted distance in $N_z = 64$ is $0.80D$ which is comparable with $0.78D$ from the experimental measurement as well as the DNS data. However, in the highest resolution in LES-4, the length is increased by 12
% between two consecutive higher resolutions of LES-3 and LES-4. This interesting or erroneous behaviour is indicating that the finer spanwise spacing itself does not automatically provide an improved result in terms of the comparison with the experiment.

The overall patterns of normalised velocity fluctuations or shear stresses $\langle u'v' \rangle / U^2$ are displayed in Figure 6(a-d). Four distinct flow clusters are visible behind the cylinder in all simulation cases and it seems that the locations of the clusters are the same as each other. The peak values of the fluctuations seem to be converged

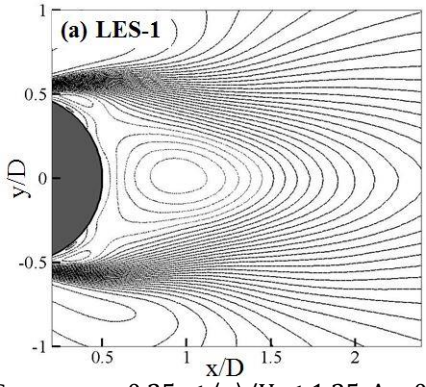

(a) Contours: $-0.25 \leq \langle u \rangle / U \leq 1.35, \Delta = 0.05$.

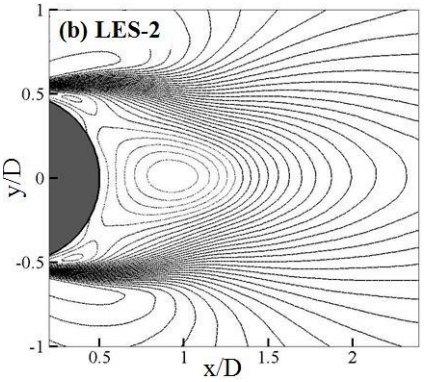

(b) Contours: $-0.25 \leq \langle u \rangle / U \leq 1.40, \ \Delta = 0.05$.

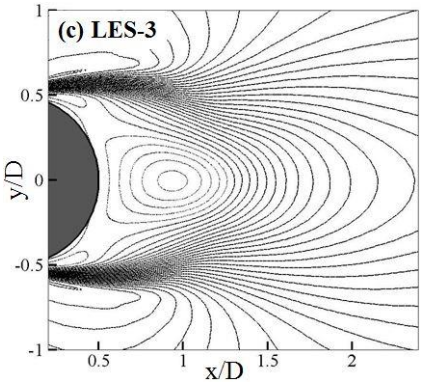

(c) Contours: $-0.25 \leq \langle u \rangle / U \leq 1.40, \ \Delta = 0.05$.

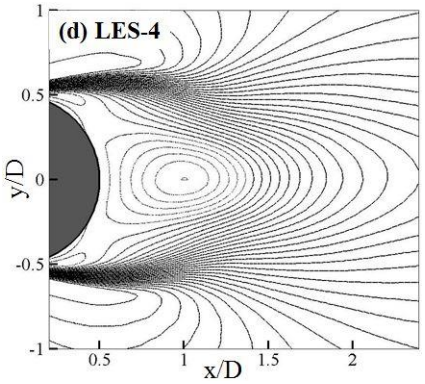

(d) Contours: $-0.30 \leq \langle u \rangle / U \leq 1.40, \ \Delta = 0.05$.

Figure 5: Contours of the spanwise-averaged mean streamwise velocity $\langle u \rangle / U$ with different spanwise resolutions.

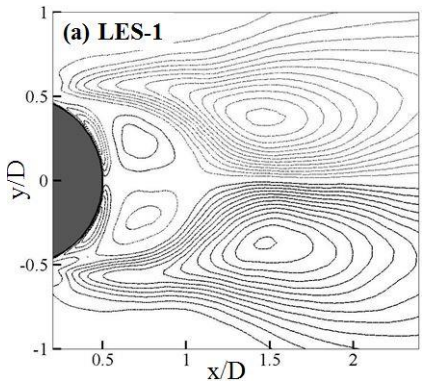

(a) Contours: $-0.13 \leq \langle u'v' \rangle / U^2 \leq 0.13,\ \Delta = 0.01$.

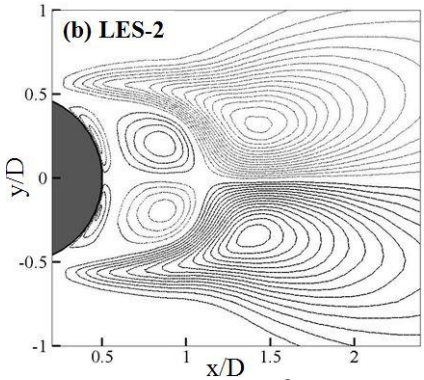

(b) Contours: $-0.16 \leq \langle u'v' \rangle / U^2 \leq 0.15,\ \Delta = 0.01$.

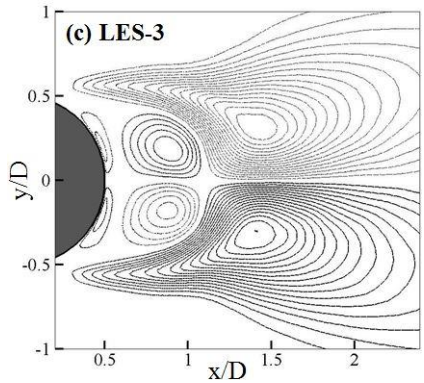

(c) Contours: $-0.17 \leq \langle u'v' \rangle / U^2 \leq 0.17,\ \Delta = 0.01$.

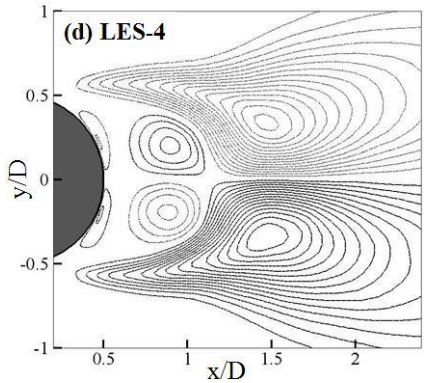

(d) Contours: $-0.15 \leq \langle u'v' \rangle / U^2 \leq 0.15,\ \Delta = 0.01$.

Figure 6: Contours of the spanwise-averaged mean shear stress $\langle u'v' \rangle / U^2$ with different spanwise resolutions.

with increasing N_z from 16 to 64, however, similarly to the behaviour of the streamwise velocity, the discrepancy of the peaks between $N_z = 64$ and 96 is above 10%. Whereas the predicted magnitude from LES-4 shows good agreement with the experiment and DNS data, the shear stress exhibits strong fluctuations with increasing the spanwise resolution.

6. CONCLUSIONS

An evaluation of the spanwise discretisation density on the unsteady near-wake flow behind the circular cylinder have been conducted at Re=10000 in the frame of 3-D LES technique. Four different spanwise resolutions were considered and all other influence parameters on LES solutions, e.g. SGS models and time resolution, were fixed for the aim of the present study. For qualitative comparison purposes, the flow variables were time- and spanwise-averaged.

Based on the comparative results of the main wake parameters for the considered high Re flow, the lift exhibited higher sensitivity as N_z increased, and the results indicated that the spanwise spacing $\Delta z/D \approx 0.05$ is required as minimum in order to predict the lift reasonably. The mean velocity profiles have been examined in near wake. The effect of the grid variations on the spanwise-averaged velocity profiles could not be definitely proved in the present study. However, the overall transversal velocity profiles showed good agreement with each other in the cases of $N_z = 64$ and 96, meaning that the grid density with at least $\Delta z/D \approx 0.05$ is necessary. Two characteristic flow distributions of the streamwise velocity and shear stress were visualised in near wake and compared with the experimental measurements. In the case of the mean velocity, the recirculation bubble length with $\Delta z/D = 0.049$ shows good agreement with the experiment, whereas the highest density with $\Delta z/D \approx 0.037$ exhibited large difference with the experiment. On the other hand, the peak value of the shear stress was improved with $\Delta z/D \approx 0.037$. This makes evaluation of LES solutions rather difficult, but the key role of the spanwise resolution on the turbulent flow is emphasised.

The present systematic study, therefore, suggests that the spatial spacing for the spanwise discretisation is necessary to satisfy $\Delta z/D \approx 0.05$ for high Reynolds number flow past a circular cylinder in order to approximate the turbulent near-wake characteristics reasonably in terms of comparison with experimental measurement.

7. ACKNOWLEDGEMENTS

The authors acknowledge the financial support from Lloyd's Register Foundation. The computations were performed on the IRIDIS-4 high performance computing cluster of the University of Southampton.

This paper was accepted after the passing way of the lead author Dr Sunghan Kim. His work and memory will remain.

8. REFERENCES

1. BEAUDAN, P. and MOIN, P., Numerical Experiments on the Flow past a Circular Cylinder at Sub-critical Reynolds Number, *Report TF-62, Stanford University, USA*, 1994.

2. MITTAL, R. and MOIN, P., Suitability of Upwind-biased Finite-difference Schemes for Large-eddy Simulation of Turbulent Flows, *AIAA Journal, Volume 35, pp 1415-1417*, 1997.

3. BREUER, M., Numerical and Modeling Influences on Large Eddy Simulations for the Flow past a Circular Cylinder, *International Journal of Heat and Fluid Flow, Volume 19, pp 512-521*, 1998.

4. JORDAN, S.A., Investigation of the Cylinder Separated Shear-layer Physics by Large-eddy Simulation, *International Journal of Heat and Fluid Flow, Volume 23, pp 1-12*, 2002.

5. PARNAUDEAU, P., CARLIER, J., HEITZ, D. and LAMBALLAIS, E., Experimental and Numerical Studies of the Flow over a Circular Cylinder at Reynolds Number 3900, *Physics of Fluids, Volume 20, 085101*, 2008.

6. MANI, A., MOIN, P. and WANG, M., Computational Study of Optical Distortions by Separated Shear Layers and Turbulent Wakes, *Journal of Fluid Mechanics, Volume 625, pp 273-298*, 2009.

7. LABBÉ, D.F.L. and Wilson, P.A., A Numerical Investigation of the Effects of the Spanwise Length on the 3-D Wake of a Circular Cylinder, *Journal of Fluids and Structures, Volume 23, pp 1168-1188*, 2007.

8. NORBERG, C., An Experimental Investigation of the Flow around a Circular Cylinder: Influence of Aspect Ratio, *Journal of Fluid Mechanics, Volume 258, pp 287-316*, 1994.

9. NORBERG, C., Fluctuating Lift on a Circular Cylinder: Review and New Measurement, *Journal of Fluids and Structures, Volume 17, pp 57-96*, 2003.

10. KIM, S., WILSON, P.A. and CHEN, Z., Numerical Simulation of Force and Wake Mode of an Oscillating Cylinder, *Journal of Fluids and Structures, Volume 44, pp 216-225*, 2014.

11. BREUER, M., A Challenging Test Case for Large Eddy Simulation: High Reynolds Number Circular Cylinder Flow, *International Journal of Heat and Fluid Flow, Volume 21, pp 648-654*, 2000.

12. WORNOM, S., OUVRARD, H., SALVETTI, M.V., KOOBUS, B. and DERVIEUX, A., Variational Multiscale Large-eddy Simulations of the Flow Past a Circular Cylinder: Reynolds Number Effects, *Computers & Fluids, Volume 47, pp 44-50*, 2011.

13. SCHUMANN, U., Subgrid Scale Model for Finite Difference Simulation of Turbulent Flows in Plane Channel and Annuli, *Journal of Computational Physics, Volume 18, pp 376-404*, 1975.

14. FUREBY, C., TABOR, H., WELLER, H.G. and GOSMAN, A.D., A Comparative Study of Subgrid Scale Models in Homogeneous Isotropic Turbulence, *Physics of Fluids, Volume 9, pp 1416-1429*, 1997.

15. ATLURI, S., RAO, V.K. and DALTON, C., A Numerical Investigation of the Near-wake Structure in the Variable Frequency Forced Oscillation of a Circular Cylinder, *Journal of Fluids and Structures, Volume 25, pp 229-244*, 2009.

16. KIM, S., WILSON, P.A. and CHEN, Z., Large-eddy Simulation of the Turbulent Near Wake behind a Circular Cylinder: Reynolds Number Effect, *Applied Ocean Research, Volume 49, pp 1-8*, 2015.

17. KIM, S., WILSON, P.A. and CHEN, Z., Effect of Turbulence Modelling on 3-D LES of Transitional Flow behind a Circular Cylinder, *Ocean Engineering, Volume 100, pp 19-25*, 2015.

18. WELLER, H., TABOR, G., JASAK, H. and FUREBY, C., A Tensorial Approach to CFD using Object Orientated Techniques, *Computers in Physics, Volume 12, pp 620-631*, 1998.

19. DONG, S., KARNIADAKIS, G.E., EKMEKCI, A. and ROCKWELL, D., A Combined Direct Numerical Simulation - Particle Image Velocimetry Study of the Turbulent Near Wake, *Journal of Fluid Mechanics, Volume 569, pp 185-207*, 2006.

20. WILLIAMSON, C.H.K., Vortex Dynamics in the Cylinder Wake, *Annu. Rev. Fluid Mechanics, Volume 28, pp 477-539*, 1996.

21. GOPALKRISHNAN, R., Vortex-induced Forces on Oscillating Bluff Cylinders, Ph.D. thesis, MIT, 1993.